Acta Crystallographica Section D
Biological Crystallography
ISSN 0907-4449

Structural elucidation of the PDI-related chaperone Wind with the help of mutants

Madhumati Sevvana,[a] Marianna Biadene,[a] Qingjun Ma,[a]‡ Chaoshe Guo,[b]§ Hans-Dieter Söling,[b]¶ George M. Sheldrick[a]* and David M. Ferrari[c]

[a]Lehrstuhl für Strukturchemie, Georg-August Universität, Tammanstrasse 4, D-37077 Göttingen, Germany, [b]Department of Neurobiology, Max Planck Institute for Biophysical Chemistry, Am Fassberg 11, Germany, and [c]Max Planck Research Unit for the Enzymology of Protein Folding, Weinbergweg 22, D-06120 Halle (saale), Germany

‡ Present address: EMBL Hamburg, c/o DESY, Notkestrasse 85, D-22603 Hamburg, Germany.
§ Present address: MCB, Harvard University, Cambridge, MA 02134, USA.
¶ Deceased 6th March 2006.

Correspondence e-mail: gsheldr@shelx.uni-ac.gwdg.de

© 2006 International Union of Crystallography
Printed in Denmark – all rights reserved

Received 12 December 2005
Accepted 22 March 2006

PDB References: Wind-His, 2c0e, r2c0esf; Y53F mutant, 2c0f, r2cofsf; Y53S mutant, 2c0g, r2cogsf; Y55K mutant, 2c1y, r2c1ysf.

The structures of the PDI-related protein Wind (with a C-terminal His_6 tag) and the mutants Y53S, Y53F and Y55K have been determined and compared with the wild-type structure with the His_6 tag at the N-terminus. All five structures show the same mode of dimerization, showing that this was not an artefact introduced by the nearby N-terminal His_6 tag and suggesting that this dimer may also be the biologically active form. Although the mutants Y53S and Y55K completely abrogate transport of the protein Pipe (which appears to be the primary function of Wind in the cell), only subtle differences can be seen in the putative Pipe-binding region. The Pipe binding in the active forms appears to involve hydrophobic interactions between aromatic systems, whereas the inactive mutants may be able to bind more strongly with the help of hydrogen bonds, which could disturb the delicate equilibrium required for effective Pipe transport.

1. Introduction

Wind, a product of the *Windbeutel* gene, is required for dorsoventral patterning in the developing embryo of *Drosophila melanogaster* along with two other gene products, Nudel (*nudel*) and Pipe (*pipe*), that constitute three of the 11 genes localized in the somatic follicle cells (Konsolaki & Schüpbach, 1997). Wind is an endoplasmic reticulum resident protein and belongs to the protein disulfide isomerase (PDI) related protein subfamily (PDI-D). PDIs are known for their varying redox and chaperone activities (Ferrari & Söling, 1999). The PDI-D group of proteins is characterized by the presence of one or two N-terminal domains of about 100–120 residues in length called the thioredoxin domain (b-domain) followed by an all-α-helical C-terminal domain about 110 residues in length termed the D-domain (Ferrari & Söling, 1999). Pipe is a Golgi-resident type-II transmembrane protein related to the vertebrate glycosaminoglycan-modifying enzyme heparan sulfate 2-*O*-sulfotransferase. It has been shown recently that Wind is required for correct targeting of Pipe to Golgi (Sen *et al.*, 2000), but the mechanism by which this process takes place is not yet understood.

The crystal structure of wild-type Wind has been described by Ma *et al.* (2003); the asymmetric unit consists of a dimer, with the dimerization-contact surface along the N-terminal b-domain. Based on this structure, a series of mutational studies have been carried out to map substrate-binding sites on the surface of Wind and a putative peptide-binding site in the Wind b-domain has been characterized with the help of *in vitro* binding assays (Barnewitz *et al.*, 2004). Within the Wind dimer, a surface tyrosine cluster formed by Tyr53, Tyr55 and

Tyr86 is important for substrate binding. Mutations at these sites (Y53S, Y55K, Y55S, Y86Q and Y86L) completely abrogate Pipe transport in *in vivo* assays. Both Y53S and Y55S are functionally inactive, whereas Y86S retains processing activity. These mutations enhance substrate binding, but reduce Pipe-processing efficiency. The Y55F mutant did not show any negative effect on Pipe processing, which further suggests that the aromatic/hydrophobic behaviour of the inner Tyr53/Tyr55 pair plays a major role in Wind–Pipe interaction. In order to assess whether structural differences are responsible for these observations, we have determined the crystal structures of the Wind Y53S, Y53F and Y55K mutants and performed some hydrophobic molecular interaction field (MIF) calculations to look at the surface hydrophobic behaviour in these mutants.

Independent mutational studies of the residues at the dimerization interface in ERp29 (a mammalian ortholog of Wind) and a preliminary low-resolution crystal structure of human ERp28 also provide a clue that the dimerization interfaces in Wind and ERp29 are similar (Lippert *et al.*, 2006). The different dimerization interface proposed on the basis of the NMR structure of the rat ERp29 monomer (Liepinsh *et al.*, 2001) may prove to have been rather speculative, as the authors themselves acknowledged.

Our original crystal structure of wild-type Wind (PDB code 1ovn) had been determined with a His_6 tag at the N-terminus (His-Wind). To rule out the possibility that the His_6 tag at the N-terminus, which is close to the dimerization region, was responsible for artefacts in the dimerization mode, we also report here the crystal structure of wild-type Wind with the His_6 tag at the C-terminus (Wind-His).

2. Materials and methods

2.1. Expression, purification and crystallization

Wild-type Wind-His protein (with the His_6 tag at the C-terminus) and the His-Wind mutants Y53S, Y53F and Y55K (with His_6 tags at the N-termini) were expressed and purified as described in Ma *et al.* (2003). Crystals of Wind-His and the mutants were obtained using the hanging-drop vapour-diffusion method (McPherson, 1992) at 293 K. The crystallization and cryoprotectant conditions are summarized in Table 1 and the crystals are shown in Fig. 1. Large crystals of Wind-His, Y53S and Y53F grew within about 4 d, whereas crystals of Y55K appeared in about a week.

Table 1
Crystallization and cryoprotectant conditions of Wind-His and its mutants.

	Wind-His	Y53S	Y53F	Y55K
Reservoir	0.1 *M* MES pH 5.8–6.6, 50 m*M* NaCl, 16–20% PEG 400	0.1 *M* MES pH 5.8–6.6, 50 m*M* NaCl, 16–20% PEG 400, 5% glycerol	0.1 *M* MES pH 5.8–6.6, 50 m*M* LiCl, 16–20% PEG 400	0.1 *M* Tris–HCl pH 8.2–8.8, 25 m*M* $MgCl_2$, 10% PEG 4000, 5% glycerol
Protein† (mg ml^{-1})	15	10	18	5
Cryoprotectant	Reservoir + 25% PEG 400, 10% glycerol	Reservoir + 25% PEG 400, 10% glycerol	Reservoir + 25% PEG 400, 10% glycerol	Reservoir + 20% glycerol

† Protein in all cases was dissolved in 5 m*M* HEPES pH 7.5, 25 m*M* NaCl, 0.0025%(*v*/*v*) β-mercaptoethanol.

2.2. Data collection and processing

The crystals of each of the mutants were soaked in a suitable cryoprotectant (Table 1) and mounted in a loop in a cold nitrogen-gas stream. The data sets were collected in two passes: a high-resolution and a low-resolution pass. The data-collection statistics are summarized in Table 2. All data sets were processed with *HKL* (Otwinowski & Minor, 1997) and the space group and data statistics were determined using *XPREP* (Bruker AXS, Madison, WI, USA).

2.3. Structure solution, refinement and validation

The Wind-His, Y53S and Y53F structures were solved by molecular replacement using *EPMR* (Kissinger *et al.*, 1999) with search models taken from the His-Wind structure (PDB code 1ovn). Monomers consisting of one b-domain and one D-domain were used, except for the solution of Y55K, for which individual b-domains and D-domains were employed. Solutions were found with correlation coefficients of 49.6, 52.5 and 51.5% for Wind-His, Y53S and Y53F, respectively. The Y55K mutant proved to be more problematic and so *PHASER* (McCoy *et al.*, 2005) was employed. First the two b-domains were located, followed by a search for the D-domains. It was only possible to locate the second D-

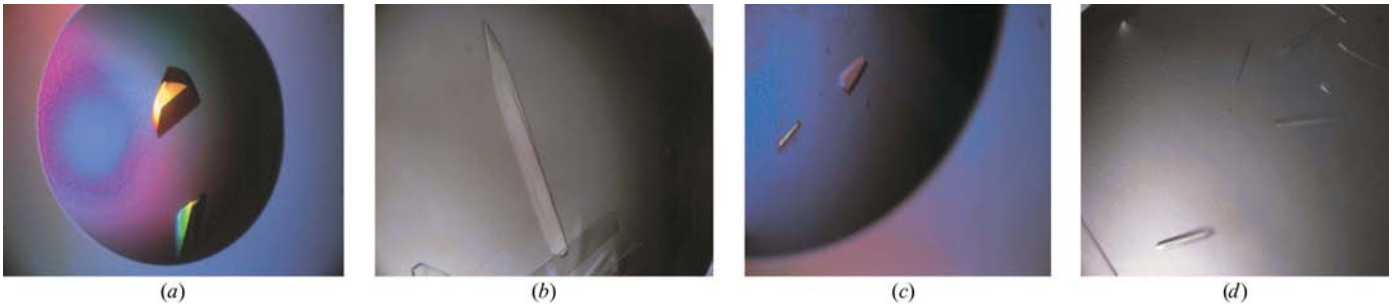

Figure 1
Crystals of (*a*) Wind-His (0.3 × 0.3 × 0.2 mm), (*b*) Y53S (0.4 × 0.1 × 0.05 mm), (*c*) Y53F (0.1 × 0.1 × 0.05 mm) and (*d*) Y55K (0.2 × 0.1 × 0.05 mm).

Table 2
Data-collection and refinement statistics.

Values in parentheses are for the outer resolution shell.

	Wind-His	Y53S	Y53F	Y55K
Data-collection statistics				
Wavelength (Å)	0.8976	0.8976	0.8976	1.0
X-ray source	BESSY BL2	BESSY BL2	BESSY BL2	DESY X13
Detector	MAR IP 345	MAR IP 345	MAR IP 345	MAR CCD
Space group	*C*2	*C*2	*C*2	$P2_1$
Unit-cell parameters				
a (Å)	107.78	108.47	109.44	35.42
b (Å)	50.36	50.55	51.71	119.09
c (Å)	98.67	98.9	100.65	64.03
β (°)	112.19	112.06	112.70	112.20
Mosaicity (°)	1.8	1.2	1.5	1.9
Resolution (Å)	2.35 (2.45–2.35)	1.75 (1.85–1.75)	2.28 (2.37–2.28)	2.25 (2.34–2.25)
Reflections (unique)	19292	47523	22333	22938
Redundancy	4.11 (3.00)	3.86 (2.96)	3.43 (3.0)	4.67 (2.62)
Completeness (%)	98.28 (99.2)	99.1 (95.9)	98.3 (89.9)	97.8 (91.2)
Mean $I/\sigma(I)$	20.05 (9.46)	19.32 (3.96)	15.19 (4.55)	16.83 (3.51)
$R_{\rm int}$† (%)	4.05 (10.87)	4.36 (26.2)	4.99 (24.32)	6.5 (26.6)
Refinement statistics				
Final *R* factor (%)				
Working set	22.60	21.92	21.92	22.27
Working + test set‡	22.95	22.15	22.24	22.63
Final free *R* factor (%)	28.34	26.75	28.06	29.25
R.m.s. deviations				
Bond lengths (Å)	0.025	0.021	0.031	0.033
Bond angles (°)	2.057	1.784	2.377	2.745
Mean *B* value (Å^2)				
Monomer 1				
Main-chain atoms	15.707	25.125	30.770	49.889
Side-chain atoms	15.313	28.175	29.646	49.065
Monomer 2				
Main-chain atoms	25.458	41.263	41.375	47.438
Side-chain atoms	22.696	37.593	38.636	46.207
Solvent	15.338	30.284	32.510	40.634
No. of protein atoms	3287	3306	3255	2699
No. of solvent atoms	108	167	98	55
PDB code	2c0e	2c0g	2c0f	2c1y

† $R_{\rm int} = \sum |F_{\rm o}^2 - F_{\rm c}^2({\rm mean})| / \sum |F_{\rm o}^2|$. ‡ 5% of reflections are selected in thin shells as the test data set.

Table 3
Dimer-interface interactions in all mutants.

The conserved interactions are shown in bold.

Mutant	Residue 1	Residue2	Distance (Å)	Charge interaction	Hydrogen bonding
His-Wind	**Gly26 N**	**Asp31 OD2**	**2.47**	**N( )···O(−)**	**Hydrogen bond**
	Asp75 OD1	**Arg41 NH2**	**2.68**	**O(−)···N(+) salt bridge**	**Hydrogen bond**
	Val28 CG1	**Val28 CG1**	**3.30**	**C( )···C( )**	
	Arg41 NH2	Lys74 O	2.80	N(+)···O( )	Hydrogen bond
Wind-His	**Gly26 N**	**Asp31 OD2**	**2.59**	**N( )···O(−)**	**Hydrogen bond**
	Asp75 OD1	**Arg41 NH2**	**2.79**	**O(−)···N(+) salt bridge**	**Hydrogen bond**
	Val28 CG1	**Val28 CG1**	**3.64**	**C( )···C( )**	
	Lys37 NZ	Thr73 O	2.71	N(+)···O( )	Hydrogen bond
	Lys37 NZ	His70 O	3.09	N(+)···O( )	Hydrogen bond
Y53S	**Gly26 N**	**Asp31 OD2**	**2.66**	**N( )···O(−)**	**Hydrogen bond**
	Asp75 OD1	**Arg41 NH2**	**2.51**	**O[−]···N(+) salt bridge**	**Hydrogen bond**
	Val28 CG1	**Val28 CG1**	**3.28**	**C( )···C( )**	
	Arg41 NH2	Lys74 O	2.85	N(+)···O( )	Hydrogen bond
	Lys37 NZ	Thr73 O	2.86	N(+)···O( )	Hydrogen bond
	Lys37 NZ	His70 O	3.01	N(+)···O( )	Hydrogen bond
	Thr73 O	Lys37 NZ	2.44	O( )···N(+)	Hydrogen bond
Y53F	**Gly26 N**	**Asp31 OD2**	**2.74**	**N( )···O(−)**	**Hydrogen bond**
	Asp75 OD1	**Arg41 NH2**	**2.38**	**O(−)···N(+) salt bridge**	**Hydrogen bond**
	Arg41 NH2	Lys74 O	2.99	N(+)···O( )	Hydrogen bond
Y55K	**Gly26 N**	**Asp31 OD2**	**2.89**	**N( )···O(−)**	**Hydrogen bond**
	Asp75 OD1	**Arg41 NH2**	**2.81**	**O(−)···N(+) salt bridge**	**Hydrogen bond**
	Val28 CG1	**Val28 CG1**	**3.76**	**C( )···C( )**	

domain with a much lower log-likelihood gain and a very low *Z* score. Though there was a solution for both the D-domains, the second D-domain had to be discarded because the *B* values were very high and there was no traceable electron density in this region during refinement. Prime-and-switch phasing in *RESOLVE* (Terwilliger, 2004) was used to minimize model bias. The model was checked and rebuilt manually from the bias-minimized electron-density map from *RESOLVE*. All structures were refined against *F* using TLS refinement in *REFMAC* (Murshudov *et al.*, 1997), alternating with model building in real space using $2mF_{\rm o} - DF_{\rm c}$ and $mF_{\rm o} - DF_{\rm c}$ maps in *COOT* (Emsley & Cowtan, 2004). The refinement statistics are summarized in Table 2. The structures were validated with *PROCHECK* (Laskowski *et al.*, 1993). All residues lie within the allowed regions of the Ramachandran plot. Figures were drawn with *CHIMERA* (Pettersen *et al.*, 2004), *MOLSCRIPT* (Kraulis, 1991) and *RASTER3D* (Merritt & Bacon, 1997).

2.4. Hydrophobic molecular-interaction field

The hydrophobic molecular-interaction fields at the surfaces of the different mutants were analysed using a DRY probe in the program package *GRID* (Goodford, 1985). The hydrophobic probe finds favourable locations that interact with other molecule(s) on the surface of a protein in an aqueous environment (Liljefors, 1998). All *GRID* calculations were performed for the whole volume of the protein using a grid spacing of 1.0 Å.

3. Results and discussion

3.1. Structure of Wind-His and its mutants

The overall fold of all three mutants is quite similar to the wild-type structure. The mutants crystallize as homodimers in the asymmetric unit, each monomer consisting of two domains, the N-terminal b-domain (118 residues) and the C-terminal D-domain (107 residues), connected by a flexible linker of

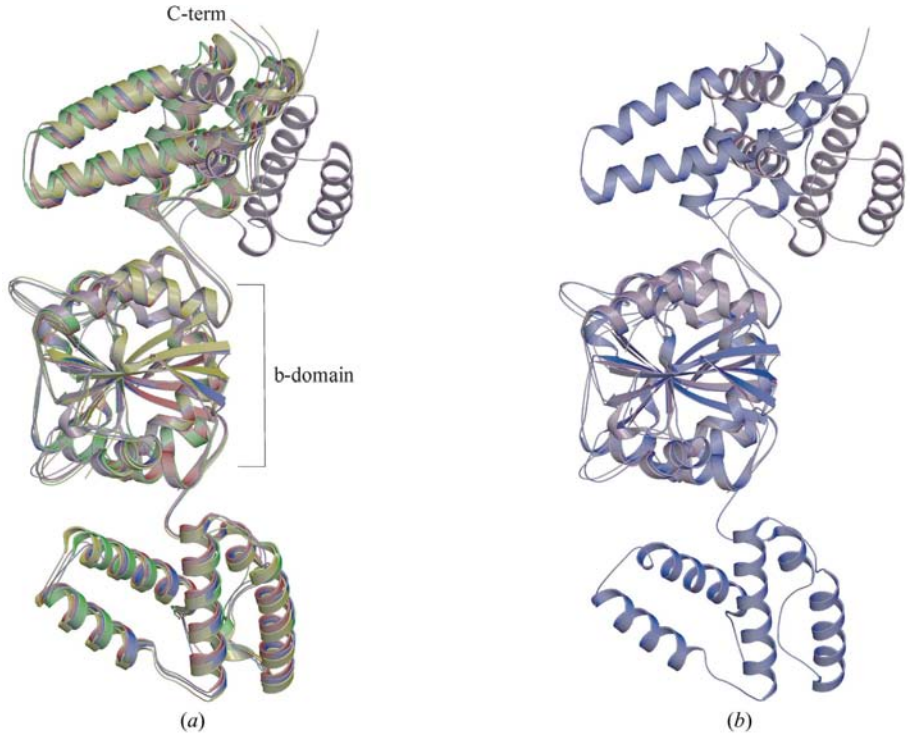

Figure 2
Superposition of dimers of (*a*) Wind-His (blue) with Y53S (green), Y53F (yellow), Y55K (plum) and His-Wind (red). (*b*) Superposition of Wind-His dimer (blue) with Y55K dimer (plum). The N-terminal b-domain and C-terminal D-domains are labelled.

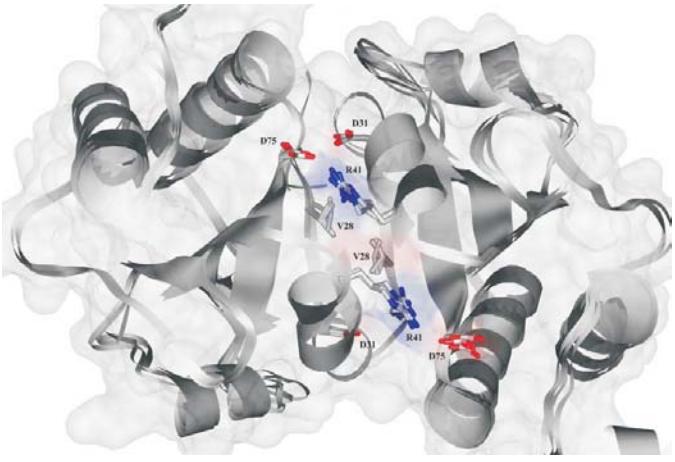

Figure 3
Superposition of the five structures viewed approximately down the non-crystallographic twofold axis of the dimer, with the key residues in the structurally strongly conserved Wind-His dimer interface highlighted.

11 residues. The b-domain adopts an α/β-fold with the order of secondary-structure elements $\beta1$-$\alpha1$-$\beta2$-$\alpha2$-$\beta3$-$\alpha3$-$\beta4$-$\beta5$-$\alpha4$. The strands of the β-sheet form a central core surrounded by the four α-helices. This fold, characteristic of protein-disulfide isomerases, is called the thioredoxin fold. The D-domain has a five-helix fold with all the helices in antiparallel arrangement. Both the N-terminal His_6 tag in the case of Y53S, Y53F and Y55K and the C-terminal His_6 tag of Wind-His were not visible in the density. The second D-domain was completely absent in Y55K.

3.2. Superposition of His-Wind and its mutants on Wind-His

Least-squares superposition of the main-chain atoms of dimers of all the mutants (Y53S, Y53F, Y55K) and wild-type His-Wind on Wind-His gave an r.m.s.d. (root-mean-square deviation) of 0.247, 0.272, 0.365 and 0.434 Å for His-Wind, Y53S, Y53F and Y55K, respectively. The program *ESCET* (Schneider, 2002) was used to determine conformationally invariant regions between different pairs of mutants. The CSI (conformational similarity index) relative to His-Wind, calculated using *ESCET*, is in the range of 90% for all the structures except for the Y55K mutant, which has a CSI of around 70%. In all the structures, the D-domains show the least significant variations, which may in part be a consequence of their higher *B* values. There are some minor differences in the loop regions of the b-domains as illustrated in Fig. 2. All the structures show significant variations in the conformations of some side chains. Compared with the other structures, the D-domain of Y55K exhibits an appreciably different orientation relative to the b-domain, with a rotation of about 45° around Gly145. With such an orientation of the D-domain with respect to the b-domain, residue Cys149 in the linker region is closer to Tyr143, with a $C^{\alpha}-C^{\alpha}$ distance between them of about 4.4 Å, compared with about 6.9 Å in the wild-type and other mutant structures. Cys149 is also closer to Tyr194 (3.65 Å) and Asn154 (3.94 Å), thus stabilizing the movement of the D-domain. The relevance, if any, of these observations with respect to a recent suggestion of a key structural role of Cys125 in rat ERp29 (homologous to Cys149 in Wind) in providing stability to the D-domain (Hermann *et al.*, 2005) remains to be established.

3.3. The dimer interface

The Wind dimer is formed by a head-to-tail arrangement of b-domains with the participation of residues constituting the $\beta1$ strand and residues within and after the $\alpha1$ and $\alpha2$ helices, mediated through a variety of hydrophobic and hydrogen-bonding interactions shown in Table 3. The partially conserved residues Gly26, Val28, Gln31 and Arg41 contribute to the dimer interface (Fig. 3). In wild-type Wind-His and all the mutants, the hydrogen-bonding distances in the region of the dimer interface agree within experimental error with those in His-Wind. The similarities in dimerization modes of Wind-His and His-Wind also indicate that the N-terminal His_6 tag in His-

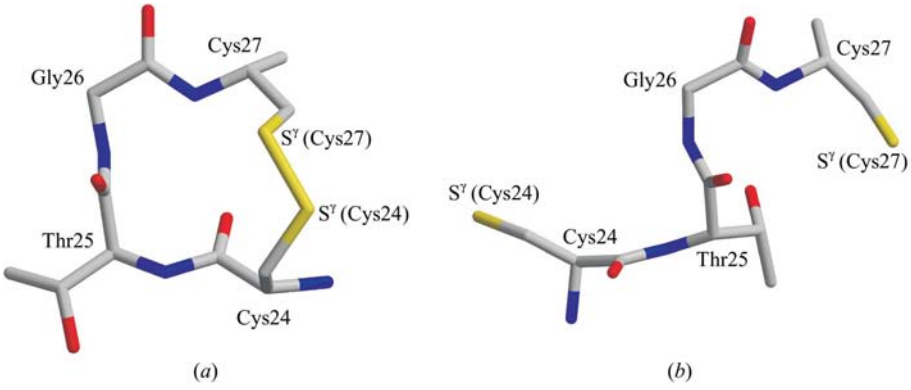

Figure 4
(*a*) Intact disulfide bond in Wind-His (His-Wind, Y53S and Y55K are similar) and (*b*) the open disulfide bridge in Y53F, which is accompanied by an approximately 180° rotation about ψ(Thr25).

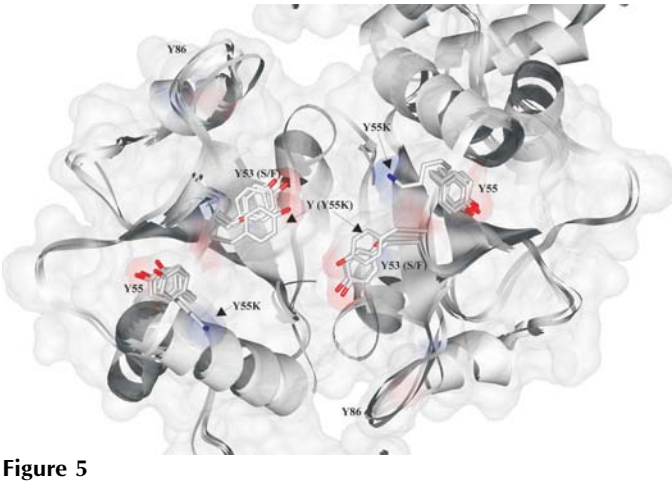

Figure 5
Superposition of the residues at the putative substrate binding site in Wind-His, His-Wind and the Y53F, Y53S and Y55K mutants. The orientations of the residues Tyr53 and Lys55 in the Y55K mutant are slightly different to those in the other four structures. The binding site stretches over both monomers and in the wild type presents a non-polar surface composed of aromatic residues at the opposite end of the non-crystallographic twofold axis of the dimer to that shown in Fig. 3.

Wind does not interfere with dimerization. The χ_1 angle of Val28 is not conserved in the mutant structure Y53F; this could be because of the changes in oxidation state of the Cys pair, which might further affect the dimerization surface and possibly the monomer/dimer ratio. In solution, Wind is present partly as a monomer but mainly as a dimer.

3.4. Opening of the CTGC loop in Y53F

In the crystal structure of Y53F, the CTGC loop in both monomers has lost its disulfide bond, as shown in Fig. 4. As a result of a change of approximately 180° in ψ(Thr25), Cys27 is about 4.2 Å from the carboxyl O atom of Glu32. The distance between Tyr53 and Cys27 is about 11.8 Å, which rules out the possibility of the mutation affecting this opening of the cysteine loop. Whether such an opening has any physiological relevance or is a consequence of radiation damage is unknown. The diffraction data did not show any other indication of radiation damage.

3.5. Substrate-binding site and hydrophobic molecular-interaction surface

The substrate-binding site of the b-domain containing the Tyr53, Tyr55 and Tyr86 residues was examined for possible structural differences amongst the mutants Y53S, Y53F and Y55K. This region is close to the pseudo-twofold axis of the dimer, so it is possible that the sites in the two monomers combine to make a single Pipe-binding site. The mutants Y53S and Y53F are conformationally very similar, but in Y55K the lysine side chain points upwards 90° away from the plane of the tyrosine ring (Fig. 5). It is possible that this results in a tighter association of the substrate (Pipe) with the Wind dimer, leading to a stronger complex, accounting for the observation in *in vivo* assays with the Wind-Y55K mutant and Pipe that Pipe translocation from Golgi was abrogated.

To analyse the hypothesis that the Wind–Pipe interaction is predominantly hydrophobic, involving aromatic interactions, the relative hydrophobic potentials on the surface shown in Fig. 6 were estimated using a DRY (hydrophobic) probe in the program *GRID* (Goodford, 1985). The net charge on each of the dimers as calculated using *GRIN* (Goodford, 1985) are −7.38, −9.05, −11.23 and −13.21 for Wind-His, Y53F, Y53S and Y55K, respectively: the two inactive mutants are appreciably more polar. In both wild-type Wind-His and the Y53F mutant, the substrate-binding site has a much larger hydrophobic interaction area at the 'tyrosine triad' than in the inactive mutants Y53S and Y55K.

3.6. Crystal-packing interactions in Y55K and Wind-His

Y55K crystallized at a different pH and in a different space group to all the other mutants and attempts to crystallize Y55K at the pH of the wild-type crystallization conditions failed, although there is no difference in dimerization mode and in the secondary structure of the b-domains. In Y55K, Tyr53 of one of the b-domains forms a hydrogen bond with Arg218 and the second Tyr53 forms a hydrogen bond with Tyr44 of a symmetry-equivalent molecule. One of the Lys55 residues forms a hydrogen bond with Ser137 of a symmetry-equivalent molecule and the second Lys55 is involved in a hydrophobic interaction with a symmetry-equivalent Phe42. In wild-type Wind-His, except for one tyrosine (Tyr55) that forms a hydrogen bond with symmetry-equivalent Arg237, all other tyrosines are involved in hydrophobic interactions. These interactions may give an indication of the differences in the substrate binding of Y55K, which has been shown to bind much more strongly than wild-type Wind-His to Pipe or to peptides derived from fragments of the Pipe sequence (Barnewitz *et al.*, 2004).

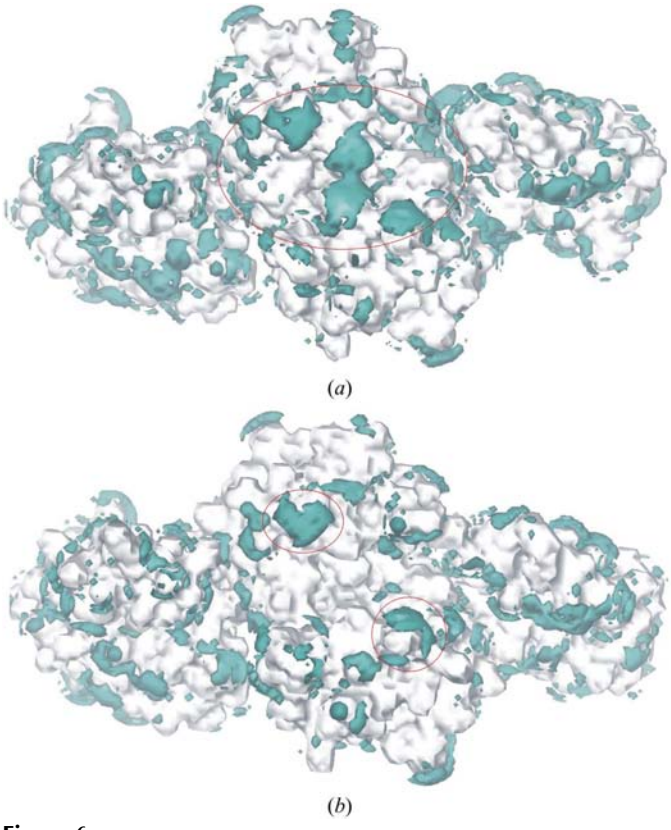

Figure 6
Hydrophobic molecular-interaction field of (*a*) the Wind-His dimer and (*b*) the Y53S dimer, contoured at -0.71 kJ mol^{-1}, highlighting the putative substrate-binding surface (encircled). For Y53F the surface is similar to (*a*) and for Y55K it is similar to (*b*).

4. Conclusions

Although the mutants Y53S and Y55K completely abrogate Pipe transport, the structural differences in the binding regions between these two mutants and the functional Y53F mutant and wild-type Wind protein in the Pipe-binding region are subtle, despite a large difference in the orientation of the b-domain and D-domain to one another in the Y55K mutant. The interactions with symmetry-equivalent molecules suggest that Y53S and Y55K may bind more strongly to Pipe, disturbing the delicate equilibrium based on predominantly hydrophobic interactions necessary for Pipe transport. The very similar structures observed for His-Wind and Wind-His indicate that the N-terminal His_6 tag, although close to the dimer interface, does not interfere with dimerization. The consistent form of dimerization for His-Wind and the four structures reported here lend support to the view that it also dominates *in vivo*, contrary to inferences based on the NMR monomer structure of a related protein, ERp29, from rat.

We are grateful to the Fonds der Chemischen Industrie, the Deutsche Forschungsgemeinschaft (SFB416) and to the European Community (Access to Research Infrastructure Action of Improving Human Potential Programme to the EMBL Hamburg Outstation, contract No. HPRI-1999-CT-000017) for support and to EMBL/DESY, Hamburg and BESSY, Berlin for generous allocations of beam time.

References

Barnewitz, K., Guo, C., Sevvana, M., Ma, Q., Sheldrick, G. M., Söling, H.-D. & Ferrari, D. M. (2004). *J. Biol. Chem.* **279**, 39829–39837.
Emsley, P. & Cowtan, K. (2004). *Acta Cryst.* D**60**, 2126–2132.
Ferrari, D. M. & Söling, H.-D. (1999). *Biochem. J.* **339**, 1–10.
Goodford, P. J. (1985). *J. Med. Chem.* **28**, 849–857.
Hermann, V. M., Cutfield, J. F. & Hubbard, M. J. (2005). *J. Biol. Chem.* **280**, 13529–13537.
Kissinger, C. R., Gehlhaar, D. K. & Fogel, D. B. (1999). *Acta Cryst.* D**55**, 484–491.
Konsolaki, M. & Schüpbach, T. (1997). *Gene Dev.* **12**, 120–131.
Kraulis, P. J. (1991). *J. Appl. Cryst.* **24**, 946–950.
Laskowski, R. A., MacArthur, M. W., Moss, D. S. & Thornton, J. M. (1993). *J. Appl. Cryst.* **26**, 283–291.
Liepinsh, E., Baryshev, M., Sharipo, A., Ingelman-Sundberg, M., Otting, G. & Mkrtchian, S. (2001). *Structure*, **9**, 457–471.
Liljefors, T. (1998). *Perspect. Drug Discov. Des.* **9**, 3–17.
Lippert, U., Sevvana, M., Söling, H. D., Sheldrick, G. M. & Ferrari, D. M. (2006). In preparation.
Ma, Q., Guo, C., Barnewitz, K., Sheldrick, G. M., Söling, H.-D., Uson, I. & Ferrari, D. M. (2003). *J. Biol. Chem.* **278**, 44600–44607.
McCoy, A. J., Grosse-Kunstleve, R. W., Storoni, L. C. & Read, R. J. (2005). *Acta Cryst.* D**61**, 458–464.
McPherson, A. (1992). *J. Cryst. Growth*, **122**, 161–167.
Merritt, E. A. & Bacon, D. J. (1997). *Methods Enzymol.* **277**, 505–524.
Murshudov, G. N., Vagin, A. A. & Dodson, E. J. (1997). *Acta Cryst.* D**53**, 240–255.
Otwinowski, Z. & Minor, W. (1997). *Methods Enzymol.* **276**, 307–326.
Pettersen, E. F., Goddard, T. D., Huang, C. C., Couch, G. S., Greenblatt, D. M., Meng, E. C. & Ferrin, T. E. (2004). *J. Comput. Chem.* **25**, 1605–1612.
Schneider, T. R. (2002). *Acta Cryst.* D**58**, 195–208.
Sen, J., Goltz, J. S., Konsolaki, M., Schüpbach, T. & Stein, D. (2000). *Development*, **127**, 5541–5550.
Terwilliger, T. C. (2004). *Acta Cryst.* D**60**, 2144–2149.